Modulation of intermembrane interaction and bending rigidity of biomembrane models via carbohydrates investigated by specular and off-specular neutron scattering

Emanuel Schneck,[1,2] Florian Rehfeldt,[2,*] Rafael G. Oliveira,[2,†] Christian Gege,[3] Bruno Demé,[4] and Motomu Tanaka[1,2,‡]
[1]*Biophysical Chemistry II, Institute of Physical Chemistry and BIOQUANT, University of Heidelberg, D69120 Heidelberg, Germany*
[2]*Department of Physics, Technical University Munich, D85748 Garching, Germany*
[3]*Department of Chemistry, University of Konstanz, D78457 Konstanz, Germany*
[4]*Institut Laue-Langevin, 6 rue Jules Horowitz, F38042 Grenoble Cedex 9, France*
(Received 26 May 2008; revised manuscript received 24 September 2008; published 30 December 2008)

We designed artificial models of biological membranes by deposition of synthetic glycolipid membrane multilayers on planar silicon substrates. In contrast to commonly used phospholipid membranes, this offers the unique possibility to study the influence of membrane-bound saccharide chains (cell glycocalix) on the membrane mechanics. Taking advantage of the planar sample geometry, we carried out specular and off-specular neutron scattering experiments to identify out-of-plane and in-plane scattering vector components. By considering the effects of finite sample sizes, we were able to simulate the measured two-dimensional reciprocal space maps within the framework of smectic liquid-crystal theory. The results obtained both at controlled humidity and in bulk water clearly indicate that a subtle change in the molecular chemistry of the saccharides strongly influences intermembrane interactions and membrane bending rigidities.

DOI: 10.1103/PhysRevE.78.061924 PACS number(s): 87.16.dj, 61.05.fg, 25.40.Dn, 87.14.Cc

INTRODUCTION

In nature, contact between cells and their surrounding tissues is mediated by hydrated biopolymers such as extracellular matrix [1] (ECM) and glycocalix [2], including various oligo- and polysaccharides. ECM is expressed in the extracellular space and consists mainly of polysaccharide chains (e.g., glycosaminoglycans, cellulose) and fibrous proteins (e.g., collagen, laminin). Glycocalix, which covers cellular plasma membranes, is composed of oligo- and polysaccharide chains bound to membrane lipids (glycolipids) and membrane proteins (glycoproteins). These saccharide layers act as "repellers" to maintain a certain distance between neighboring cells, and create hydrodynamic pathways for the diffusion of ions and molecules [3]. In the case of Gram-negative bacteria, they can act as protection against the environment and prevent the permeation of antimicrobial peptides [4]. In order to physically model interactions at soft biological interfaces (electrostatic interactions, long-range van der Waals interactions, hydrogen bonding, and entropic interactions), it is essential to design well-defined model systems with a reduced number of components.

To date, the physical characteristics of phospholipid bilayers, the basic structuring component of biological membranes, have been studied intensively using x-ray and neutron scattering. In contrast to commonly used powder diffraction experiments on lipid suspensions, the planar geometry of solid-supported multilayers allows for the identification of in-plane and out-of-plane momentum transfers [5,6]. Information on the structure normal to the sample plane can be obtained from specular scattering, whereas information on the structural ordering parallel to the sample plane (reflecting the mechanical properties of interacting model membranes) can be extracted from off-specular signals. Due to these advantages, solid-supported membrane multilayers have been widely used to study the behavior of interacting phospholipid membranes in many aspects [7–11]. However, phospholipid membranes are only of limited use to model cell-cell contacts, and thus more realistic model systems, mimicking the oligosaccharide-rendered surfaces of cells and bacteria, are required.

In the present paper we studied solid-supported multilayers of synthetic glycolipid membranes by specular and off-specular neutron scattering to examine the influence of the saccharide head group conformation on their structural ordering and mechanical properties. The samples were placed either in a temperature-controlled climate chamber for experiments under various relative humidities, or in a liquid cell for experiments in bulk water to ensure full hydration.

MATERIALS AND METHODS

Chemicals, sample preparation

The structures of the synthetic glycolipids used in this study are given in Fig. 1. All the lipids consist of two saturated hexadecyl chains and a disaccharide head group, connected to the alkyl chains via a glycerol junction. Gent lipid has a gentiobiose head group [*O*-(*β*-*D*-*glucopyranosyl*)-(1→6)-*β*-*D*-*glucopyranoside*], which is bent with respect to the molecular axis. On the other hand, Lac1 lipid has a cylindrical mono-lactose [*O*-(*β*-*D*-*galactopyranosyl*)-(1→4)-*β*-*D*-*glucopyranoside*] head group. For optimizing the contrast in scattering length density (contrast variation), we

*Present address: Georg-August-Universität, III. Physikalisches Institut, 37077 Göttingen, Germany.
†Present address: CIQUIBIC-UNC, Ciudad Universitaria X5000HUA, Córdoba, Argentina.
‡Author to whom correspondence should be addressed: tanaka@uni-heidelberg.de

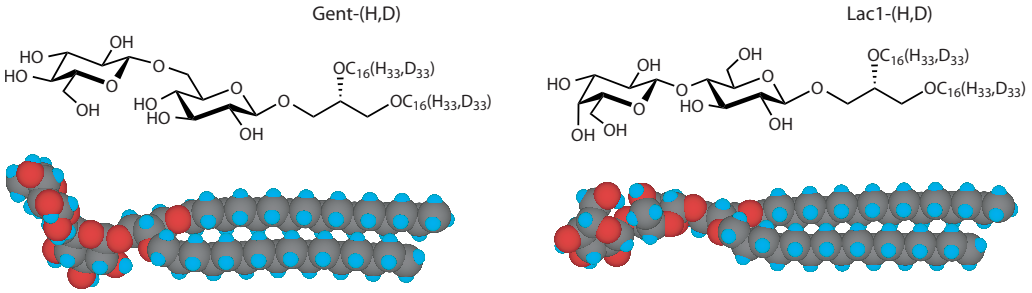

FIG. 1. (Color online) Chemical structures and space-filling models of the glycolipids used in this study. The Gent lipid (left) has a "bent" gentiobiose head group, while the Lac1 lipid (right) has a "cylindrical" lactose head group.

used molecules with fully hydrogenated alkyl chains (Gent-H, Lac1-H) as well as those with fully deuterated chains (Gent-D, Lac1-D). The deuterated membrane anchor was synthesized as described for the nondeuterated derivative [12] by reaction of 1-*O*-benzyl-*sn*-glycerol with excess 1-bromohexadecane-d33 (ABCR, Karlsruhe, Germany) and subsequent hydrogenolytic *O*-debenzylation. This deuterated membrane anchor was coupled to the carbohydrate moiety as previously described for Lac1-H [13] and Gent-H [14] to give Lac1-D and Gent-D, respectively. All the other chemicals were purchased from Fluka (Taufkirchen, Germany) and used without further purification.

The molecules were dissolved in 7:3 mixtures (v/v) of chloroform and methanol at a concentration of 1 mg/mL. 1–2 mL of this solution were deposited onto Si(100)-substrates with native oxide (Si-Mat, Landsberg/Lech, Germany), which were cut into a rectangular shape (65 mm $\times$25 mm) and cleaned by a modified RCA method [15]. Due to their amphiphilic nature, the glycolipid molecules form thin films of bilayer membrane stacks, which are aligned parallel to the substrate surface. Depending on the amount of solution, the average number of membranes in the stacks ranges from 500 to 1000. To remove residual solvent, the coated wafers were stored at 70 °C for 3 h, and subsequently in a vacuum chamber overnight. At least two heating/cooling cycles between 20 and 80 °C were performed at a high relative humidity ($h_{\mathrm{rel}}>95\%$) to cancel the thermal history of the samples prior to the measurements. For maximum scattering contrast, D_2O was used to hydrate molecules with hydrogenated alkyl chains, while H_2O was used for molecules with deuterated alkyl chains.

Neutron scattering

Neutron scattering experiments were carried out at the D16 membrane diffractometer of the Institut Laue-Langevin (ILL, Grenoble, France). A monochromatic neutron beam ($\Delta\lambda/\lambda=1\%$) of $\lambda=4.54$ Å reaches the sample through the aluminum windows of the sample chamber, while the incident angle Ω (i.e., the angle between the incident beam and the sample plane) is adjusted by a rotation stage. The intensity of the beam diffracted from the sample is recorded by a position sensitive ^{3}He 2D detector with 128×128 channels. Figure 2 (left) shows the geometry of the experiment (top view). Γ denotes the angle between the scattered and the incident beam. The sample was rotated stepwise with respect to the incident beam. The beam width was 2 mm horizontally and 25 mm vertically. For each measurement at an angle Ω, the detector readout was normalized to the intensity of the incident beam (via an in-beam monitor), the channel sensitivity, and the illuminated sample area. Subsequently, the two-dimensional (2D) detector readout was integrated in the vertical direction, which results in a one-dimensional intensity projection as a function of the horizontal detector channel position (corresponding to Γ). Thus, one Ω scan yielded the recorded intensity as a function of Ω and Γ. Figure 2 (inset right) shows a typical rocking scan around the second Bragg peak. The width of the central specular maximum is approximately 0.1 degrees and indicates a remarkable alignment of the multilayers to the flat substrate. The datasets in angular coordinates can be transformed into reciprocal space maps (Fig. 2, right) by geometrical considerations,

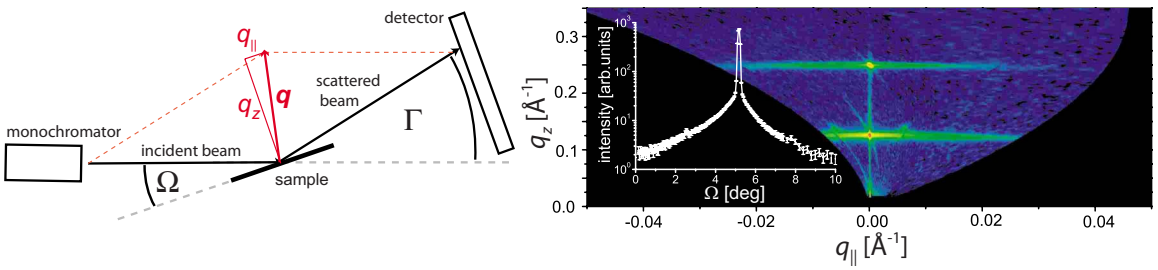

FIG. 2. (Color online) Left: Geometry of the scattering experiments. The reciprocal space coordinates (i.e., the scattering vector components q_z and $q_\parallel$) are functions of Γ and Ω [Eqs. (1)]. Right: (main panel) Measured reciprocal space map from Gent-D lipid membranes at 80 °C and relative humidity $h_{\mathrm{rel}}\sim95\%$, plotted as a function of q_z and $q_\parallel$. The central vertical line corresponds to a specular condition ($\Gamma=2\ \Omega$), while the horizontal stripes resulting from the sample periodicity are known as Bragg sheets. (Inset) Typical rocking scan around the second Bragg peak indicating the high alignment of the membrane multilayers to the substrate.

$$q_z = \frac{2\pi}{\lambda}[\sin(\Gamma - \Omega) + \sin(\Omega)],$$

$$q_\parallel = \frac{2\pi}{\lambda}[\cos(\Gamma - \Omega) - \cos(\Omega)]. \quad (1)$$

Here, q_z and $q_\parallel$ denote the scattering vector components perpendicular and parallel to the sample plane (see Fig. 2, left), i.e., the coordinates of the reciprocal space. It should be noted that data could be recorded not only in reflection ($\Omega > 0$ and $\Gamma - \Omega > 0$) but also in transmission, due to the weak neutron absorption of silicon.

Sample environments

The main phase transition temperatures of Lac1 lipid (T_m=74 °C) and Gent lipid (T_m=43 °C) have previously been measured by differential scanning calorimetry (DSC) and small- and wide-angle x-ray scattering (SAXS and WAXS) [16,17]. To study the influence of molecular structures on structural ordering and mechanical properties of the stacked membranes, a temperature at which both molecules are in L_α phase was chosen (T=80 °C).

Climate chamber

For measurements at controlled relative humidity, the ILL setup for temperature and humidity control was used [18]. The climate chamber consists of two cells: a sample chamber and a chamber containing a reservoir for liquid water. The cells are thermally isolated but interconnected for vapor exchange. Two independent thermostats (Phoenix II, Haake, Karlsruhe, Germany, ΔT=0.1 °C), controlled by the instrument control program, regulate the temperatures in the sample chamber T_s and the water reservoir T_r, which allows for the regulation of both sample temperature and relative humidity (i.e., the osmotic pressure exerted to the sample, defined by the chemical potential of water vapor in equilibrium) in the chamber. The relative humidity in the sample chamber, h_{rel}, can be given as a function of T_r and T_s,

$$h_{\mathrm{rel}}(T_r) = p(T_r)/p(T_s). \quad (2)$$

$p(T_s)$ and $p(T_r)$ denote the saturation water vapor pressures in the sample and reservoir chambers, respectively. Here, the osmotic pressure [19] p_{osm} exerted to the sample is given by van t' Hoff's law. At thermal equilibrium, the disjoining pressure [20,21] p_{dis} counterbalances the osmotic pressure,

$$p_{\mathrm{dis}} = -p_{\mathrm{osm}}(T_r) = -\frac{k_B T_s}{V_{\mathrm{water}}} \ln[h_{\mathrm{rel}}(T_r)], \quad (3)$$

where V_{water} denotes the molecular volume of water, and k_B is the Boltzmann constant. To ensure the equilibration, the sample was kept at each temperature and humidity condition for at least 30 min before the measurement.

Liquid cell

For experiments in bulk water, a self-built liquid cell was used [18]: It consists of two rectangular Si wafers (65 mm × 25 mm), one of which is coated with the membranes. The wafers are separated by glass slide pieces (thickness: 0.10 mm). The capillary force confines a thin layer of aqueous solution between the two wafers. During measurements, the entire liquid cell was placed in the climate chamber at controlled temperature and high relative humidity (>95%) to avoid the evaporation of water. Owing to the high incoherent scattering of H_2O and the lower transmission of neutrons through the water, measurements with a liquid cell were carried out on hydrogenated glycolipids in D_2O.

THEORY AND DATA MODELING

Discrete smectic hamiltonian

Within the framework of a continuum model approximation, the total free energy of membrane stacks can be described with the discrete smectic Hamiltonian [22] H,

$$H = \int_A d^2 r \sum_{n=1}^{N-1} \left(\frac{B}{2d}(u_{n+1} - u_n)^2 + \frac{\kappa}{2}(\nabla_{xy}^2 u_n)^2 \right). \quad (4)$$

N is the total number of membranes, d their equilibrium distance, A the covered area, and u_n the local out-of-plane displacement of the nth membrane from its average vertical position. Within this framework, vertical compression is characterized by the compression modulus B, while bending is characterized by the membrane bending modulus κ. ∇_{xy} denotes the two-dimensional Nabla operator in x and y directions.

Membrane displacement correlation functions

For stacks of membranes that are infinitely expanded in all directions, the out-of-plane membrane displacement correlation function $g_k(r)$ between a membrane and its kth nearest neighbor can be expressed with the Caillé parameter η and the de Gennes parameter λ of smectic liquid crystals [22],

$$g_k(r) := \langle [u_{n\pm k}(\vec{r}_0 + \vec{r}) - u_n(\vec{r}_0)]^2 \rangle_{\vec{r}_0} = \frac{d^2}{\pi^2}\eta \int_0^\infty f_k dq_\parallel, \quad (5)$$

with

$$f_k = \frac{[1 - J_o(q_\parallel r)\exp(-\lambda k q_\parallel^2 d)]}{q_\parallel \sqrt{1 + \frac{\lambda^2 d^2}{4} q_\parallel^4}}, \quad \eta = \frac{\pi k_B T}{2d^2\sqrt{\kappa B/d}},$$

$$\lambda = \sqrt{\frac{\kappa}{Bd}}, \quad r = |\vec{r}|.$$

Here, $q_\parallel$ denotes the reciprocal space coordinate parallel to the membrane plane [see also Eqs. (1)]. In the case of infinitely expanded membrane stacks, the displacement correlation functions diverge with increasing lateral distance r, resulting in an infinite root-mean-square (rms) roughness. However, this is not realistic for membrane multilayers on planar solid substrates, where fluctuations of long wavelengths are suppressed due to the finite sample size. Thus, to model a system with finite rms roughness, we introduced a

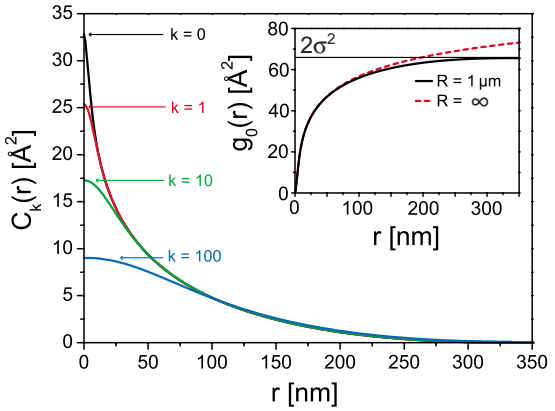

FIG. 3. (Color online) Membrane displacement correlation functions $C_k(r)$, plotted for a given set of parameters: η=0.04, λ =20 Å, R=1 μm. Inset: $g_0(r)$ for the same values of η and λ, in the infinite case (R=∞), and in the finite case (R=1 μm), where the curve saturates to the finite value $2\sigma^2$.

lower integration limit, $2\pi/R$, in the displacement correlation functions,

$$g_k(r) = \frac{d^2}{\pi^2}\eta\int_{2\pi/R}^{\infty} f_k dq_\parallel. \tag{6}$$

Previously, Lei *et al.* used an upper integration limit in the scattering intensity calculation to model specular scattering signals from surfactant multilayers [22], which is mathematically analogous to our approach. Here, the free parameter R, the effective cutoff radius, accounts for two effects: (i) The finite lateral size of the membrane patches acts as an upper limit for the wavelength at which the membranes can fluctuate. (ii) Long-wavelength membrane fluctuations are more collective (i.e., they involve more layers) and are therefore damped more strongly by the flat solid support in samples with a finite number of layers [23]. The consequence of the cutoff radius is illustrated in Fig. 3 (inset), where $g_0(r)$ is shown for given η and λ in the infinite case (R=∞) and in the finite case (R=1 μm), where the curve saturates to the finite value $2\sigma^2$. Only by introducing the lower integration limit $2\pi/R$ are we able to compute the full set of correlation functions necessary for the simulation of the measured two-dimensional reciprocal space maps including specular and off-specular parts in a quantitative manner. This is thus advantageous over previous approaches, where mechanical properties were calculated either from the power-law decays or from the numerical back-transformations of integrated Bragg sheet intensities [7]. The method we present allows for the full description of the measured scattering signals with the continuum-mechanical parameters B and κ.

To model the scattering signals, the displacement correlation functions can be rewritten in another form, $C_k(r)$, based on the finite rms roughness σ,

$$C_k(r) := \langle u_{n\pm k}(\vec{r}_0+\vec{r})\cdot u_n(\vec{r}_0)\rangle_{\vec{r}_0} = \sigma^2 - g_k(r)/2. \tag{7}$$

Such a set of correlation functions (k=0,1,10,100) for given, η, λ, and R is also shown in Fig. 3 (main panel).

Simulation of the scattering signals

To simulate the scattering signals, we use the first Born approximation, which assumes that scattering is weak compared to the incident illumination. In the following, we therefore consider only the second Bragg sheets, where the validity of the first Born approximation is guaranteed. In this approximation, the scattering from a set of stratified interfaces with correlated roughness is given by [24]

$$S(q_z,q_\parallel) \propto \frac{1}{q_z^2}\sum_{n,m=0}^{N} e^{-(1/2)q_z^2(\sigma_n^2+\sigma_m^2)}\Delta\rho_n\Delta\rho_m e^{-iq_z(z_n-z_m)} \times \int_{-\infty}^{\infty} e^{q_z^2 C_{nm}(r)} e^{-iq_\parallel r} dr. \tag{8}$$

N denotes the total number of stratified interfaces, $\Delta\rho_n$ is the step in scattering length density across the nth interface, and C_{nm} is the cross-correlation function between the nth and the mth interface. In the case of membrane multilayers with constant membrane periodicity, Eq. (8) can be simplified: $|z_n - z_m| = kd$, and $\Delta\rho_n \to \Delta\rho$. It is also plausible to ignore the different behavior of the layers close to the upper and bottom boundaries, since the scattering signals are vastly dominated by the bulk membrane stacks [7], i.e., $C_{nm}(r) \to C_k(r)$ and $\sigma_n \to \sigma$. Thus, we can directly use the displacement correlation functions derived in Eqs. (6) and (7) for further considerations,

$$S(q_z,q_\parallel) \propto \frac{e^{-q_z^2\sigma^2}}{q_z^2}\left[N + 2\sum_{k=1}^{N}(N-k)\cos(kq_z d) \times \int_{-\infty}^{\infty} e^{q_z^2 C_k(r)} e^{-iq_\parallel r} dr\right]. \tag{9}$$

To maintain a uniform grid of points in experimental and simulated datasets, the scattering signals were modeled in the angular coordinates of the experiment. It should be noted that the data measured at very small angles near the critical angle of incidence (Yoneda wings [25]) cannot be used when we compare the theoretical models and the scattering signals, because Eqs. (1) become erroneous due to refraction. For the calculations in Eq. (9) we used N=100, which was found to be sufficient to generate model signals much sharper than the instrumental resolution. Figure 4 presents the comparison of a measured (left) and the corresponding simulated (right) second Bragg sheet. Instrumental resolution was included by convolution of the signal in the Ω and Γ directions with a Gaussian function, representing the point spread function of the measurement as it results from the finite angular width and the wavelength spread of the neutron beam: the convolution in the Ω direction was achieved using the Fourier convolution theorem in the computation of the Fourier integrals in Eq. (9), while the convolution in the Γ direction was applied to the simulated intensity maps. In the simulations, the parameters η, λ, and R were varied to find the best accordance with the experimental data. Moreover, the importance of the correct choice of the effective cutoff radius R is illustrated in Fig. 6 (inset, top right panel), where simulations

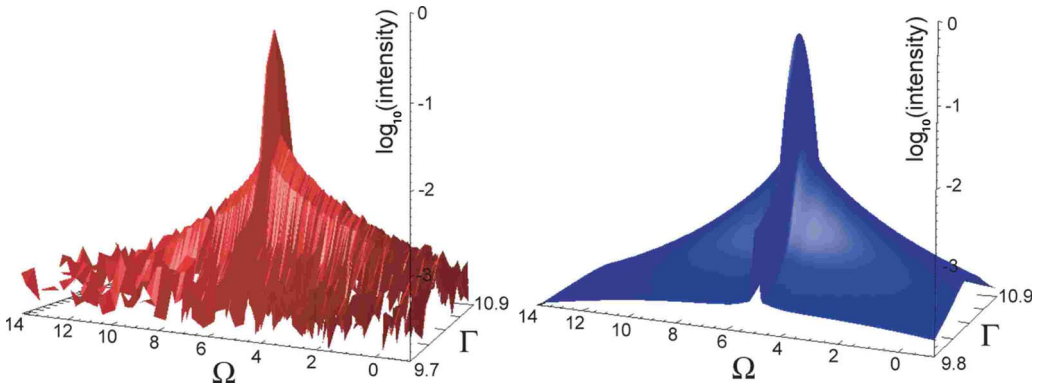

FIG. 4. (Color online) Scattering intensity of the second Bragg sheet as a function of the angles Ω and Γ. Left: experimental data; right: simulation. System: Gent-D in H_2O atmosphere at $T=80\,^{\circ}C$ and $h_{rel}\sim 95\%$.

based on three different values of R are compared to the experimental scattering intensities.

RESULTS AND DISCUSSION

Intermembrane interactions

The lamellar periodicity d of the glycolipid multilayers can be calculated from the positions of the Bragg peaks under defined temperature and humidity conditions. At 80 °C and high relative humidity (~95%), the periodicity of Gent-D multilayers is $d=50.1$ Å, while the corresponding value for Lac1-D is $d=56.5$ Å. The difference in membrane periodicity seems to reflect the difference in the projected length of the carbohydrate head groups normal to the membrane plane. Measurements of the lamellar periodicity d at various osmotic pressures (in this study, $p_{osm}=5\times10^6$ Pa-3×10^8 Pa, corresponding to $h_{rel}=97-15$ %) enabled the determination of quantitative relationships between the membrane periodicity and the disjoining pressure (i.e., the net interfacial force per unit area), referred to as *force-distance relationships*. In contrast to the so-called osmotic stress method, where impermeable solutes (e.g., water soluble polymers impermeable across the membrane) are utilized to create a low external osmotic pressure ($p_{dis}<10^6$ Pa) in bulk solvents [26,27], measurements at vapor pressures (i.e., in the absence of condensed water) allow for the precise control of the disjoining pressure at high values ($p_{dis}>10^6$ Pa), without the risk of sample contamination by additional solutes. Force-distance relationships indeed enabled the identification of interaction regimes governed by different dominant force contributions. The forces applied in this study covered a high-pressure regime ($>\sim5\times10^7$ Pa) dominated by steric forces, which can be described by a power law [$p_{steric}(d)\sim d^{-(n+1)}$, $9<n<16$], and a regime dominated by hydration forces [28], following an exponential decay at lower pressures ($<\sim5\times10^7$ Pa),

$$p_{hydr}(d)\propto e^{-d/\lambda_{hydr}}. \tag{10}$$

The force-distance relationships (p_{dis} vs d) of Gent-H and Lac1-H multilayers at 80 °C are presented in a semilogarithmic plot in Fig. 5. Here, the horizontal error bars correspond to the experimental errors of the periodicity measurement from the instrumental resolution, while the vertical ones coincide with the uncertainties of the relative humidity in the climate chamber. The dashed and solid lines show the models fitted to the data points within the two pressure regimes. Note that the shape of the power law is almost indistinguishable from a straight line in the semilogarithmic presentation

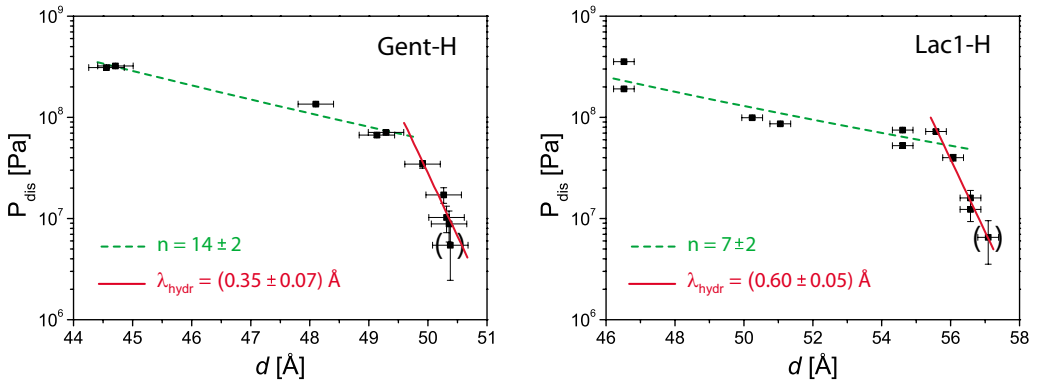

FIG. 5. (Color online) Force-distance curves of Gent-H (left) and Lac1-H (right), obtained from measurements of the lamellar periodicity at different relative humidities at 80 °C. Two different regimes can be identified: Steric repulsion at higher pressures ($>\sim5\times10^7$ Pa) and a second regime (see text for details) at lower pressures ($<\sim5\times10^7$ Pa). The dashed and solid lines correspond to the models fitted to the data points within the two pressure regimes.

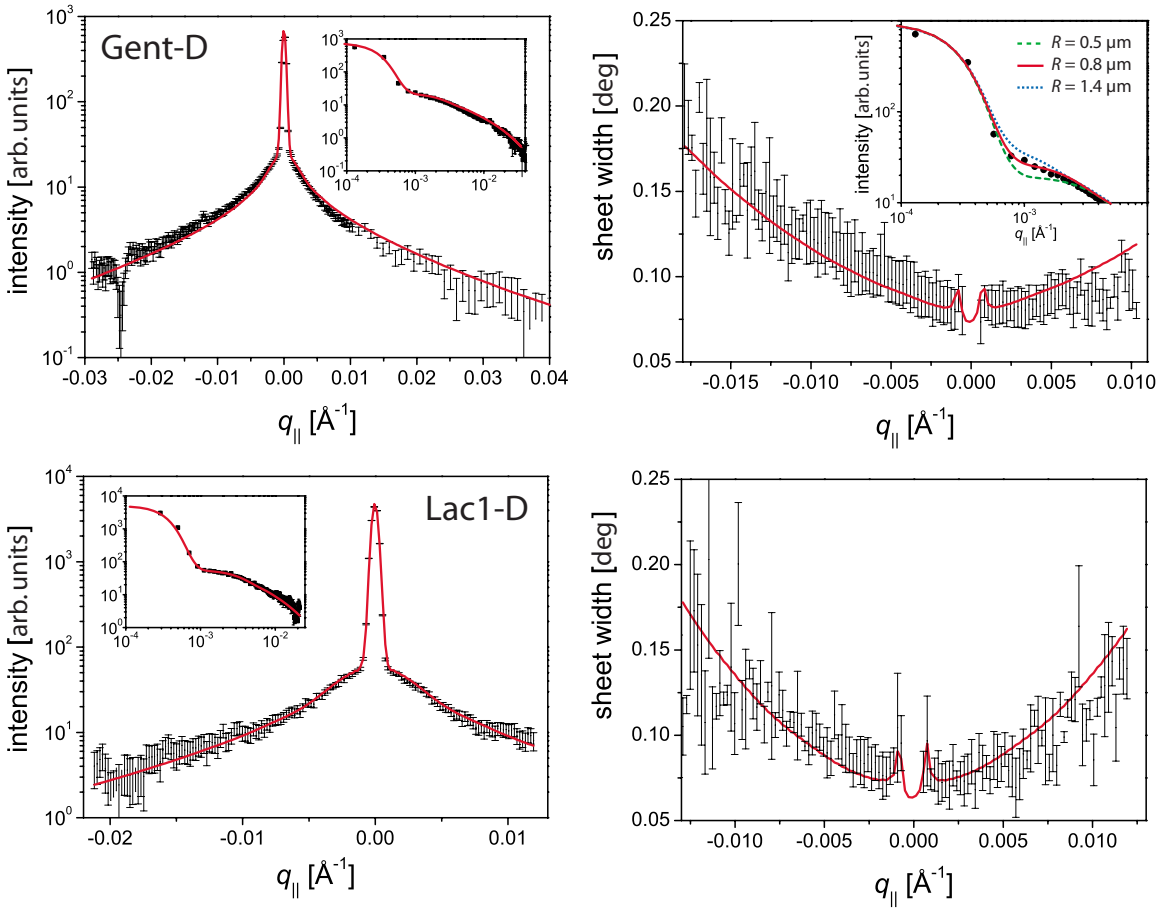

FIG. 6. (Color online) Measured (data points) and simulated (solid line) second Bragg sheets of Gent-D (top) and Lac1-D (bottom) membrane multilayers at 80 °C and $h_{rel} \sim 95\%$. Left column: Intensity integrated along Γ plotted as a function of $q_{||}$ (inset: log/log plot). Right column: width of the sheet along Γ as a function of $q_{||}$. Inset top right panel: Comparison of experiment (data points) and simulation (lines) for three different values of the cutoff radius R.

due to the limited range of the d axis. In the high-pressure regime, Gent-H exhibits a characteristic exponent of $n = 14 \pm 2$, which is within the typical range to describe steric forces. In contrast, the value of Lac1-H ($n = 7 \pm 2$) is smaller, indicating that the steric repulsion between the opposing head groups is weaker. This can be attributed to the difference in the finite compressibility of cylindrical lactose head groups and bent gentiobiose head groups in the direction normal to the membrane surface. At lower pressures, the characteristic decay lengths obtained for both glycolipids [Gent-H: $\lambda_{hydr} = (0.35 \pm 0.07)$ Å and Lac1-H: $\lambda_{hydr} = (0.60 \pm 0.05)$ Å] are significantly lower than those reported for phosphocholine membranes (~2 Å [27,29]), indicating that neighboring glycolipid membranes are coupled more strongly than phospholipid membranes, possibly due to additional attractive force contributions (such as "zipper" forces between carbohydrates) that compete with the hydration repulsion.

A recent account reported that specular neutron scattering measurements at several osmotic pressures are possible for stacks of bacterial lipids [30]. However, to gain insight into the force interplay at zero osmotic pressure [27,31], experiments in bulk water are desirable.

Mechanical properties

As described in the Theory section, the parameters η, λ, and R are varied in the simulations to achieve the best match

TABLE I. Parameters of the best matching simulations for Gent-D and Lac1-D membranes at $T = 80$ °C and $h_{rel} \sim 95\%$.

System	d (Å)	σ (Å)	η	λ (Å)	R (μm)	κ (J)	κ (k_BT)	B (MPa)
Gent-D	50.1	3.5	0.023	6	0.8	3.9×10^{-20}	8	21
Lac1-D	56.5	2.6	0.011	13	0.5	1.6×10^{-19}	32	17

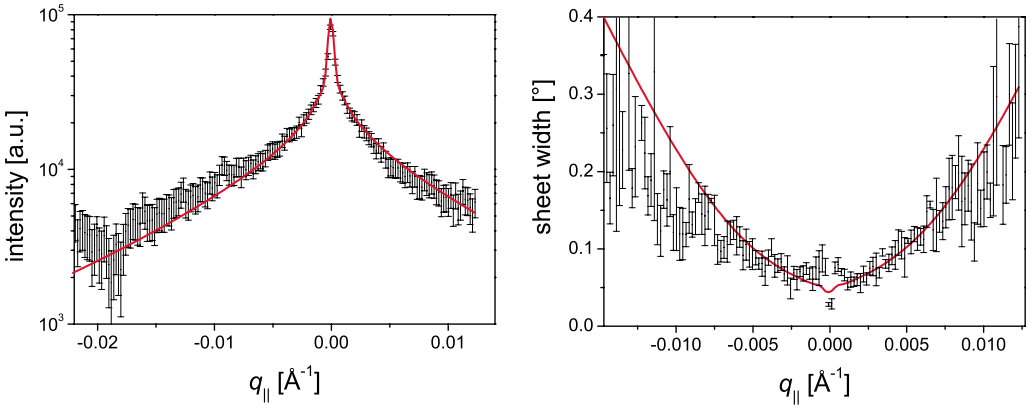

FIG. 7. (Color online) Measured (data points) and simulated (solid line) second Bragg sheet of Gent-H membrane multilayers at 60 °C in bulk D_2O. Left: intensity integrated along Γ plotted as a function of $q_{\|}$. Right: width of the sheet along Γ as a function of $q_{\|}$.

to the experimental data, which enables us to calculate the compression modulus B and the bending modulus κ. To compare the measured datasets with the simulations, two representations are selected: (i) measured and simulated intensity of the second Bragg sheet integrated along Γ plotted as a function of $q_{\|}$. (ii) Measured and simulated width of the Bragg sheet along Γ presented as a function of $q_{\|}$.[1] The first representation reflects the displacement self-correlation $C_0(r)$ of the stacked membranes, while the second one reflects the value of the de Gennes parameter λ. Figure 6 shows the measured (black data points) and simulated (solid red line) second Bragg sheets of Gent-D and Lac1-D membranes. For both systems, the experiments were carried out at 80 °C and at high relative humidity ($h_{\mathrm{rel}} \sim 95\%$). Note that the simulations based on parameter sets summarized in Table I agree well with experimental results in both representations.[2] The optimal R values are in the range of 1 μm, which shows reasonable agreement with the actual size of the multilayer domains determined by AFM measurements [18]. The obtained bending moduli have the same order of magnitude as those reported [32,33] for phospholipids with similar chain lengths in the L_α phase. However, the bending modulus we found for Lac1-D membranes ($\kappa \sim 32 k_B T$) is significantly higher than that for Gent-D membranes ($\kappa \sim 8 k_B T$), suggesting that cylindrical lactose head groups resist the bending of the membranes much more than "bent" gentiobiose head groups. This seems to coincide with our previous studies, where we found that Lac1 lipids even form physical gels of ordered head groups [14,34,35]. The obtained intermembrane compression modulus of Gent-D membranes, $B = 21$ MPa, is slightly higher than that of Lac1-D membranes ($B = 17$ MPa), indicating that the intermembrane confinement of Lac1-D membranes is softer than that of Gent-D membranes. The obtained results demonstrate that the approach taken in this study offers a powerful tool to identify the effects of subtle changes in molecular structures on the intermembrane interactions and mechanical properties of biomembrane models.

[1]It can be shown [36] that the intensity of the Bragg sheets, integrated along q_z, depends only on the displacement self-correlation function $C_0(r)$. Furthermore, the width in q_z of the Bragg sheets scales with $q_{\|}^2$ with a prefactor proportional to the de Gennes parameter λ. To avoid integrations and peak fitting in the nonuniform grid of data points in the reciprocal space coordinates (Fig. 2, right), we calculate integrated intensities and sheet widths in angular coordinates and present them as a function of $q_{\|}$ (Fig. 6).

[2]The relative accuracies of the three parameters are discussed in the EPAPS material [18]. The uncertainties of B and κ follow from the uncertainties of η and λ according to Gaussian error propagation.

Measurements in bulk water

To study the intermembrane interaction and bending rigidity of the glycolipid membranes in the absence of external osmotic pressures, we carried out experiments on Gent-H membranes in bulk D_2O at 60 °C using a self developed-liquid cell. The thermal stability of the sample in bulk D_2O during the measurement can be verified by the symmetry of the Bragg sheets in the Ω direction, since the Ω axis is proportional to the time axis in a rocking scan. From the Bragg peak positions, the periodicity of the Gent-H membrane multilayers was determined to be $d = 56.8$ Å, which is in good agreement with the value obtained by SAXS at 70 °C, $d = 58$ Å [16]. Figure 7 shows the measured and simulated second Bragg sheet and the parameters corresponding to the best model are presented in Table II.

Interestingly, the obtained bending modulus ($\kappa_{\mathrm{bulk}} = 7 k_B T$) is similar to that obtained at $h_{\mathrm{rel}} \sim 95\%$, $\kappa_{\mathrm{vapor}} = 8 k_B T$, indicating that the work required to bend the membrane is not influenced significantly by the presence of bulk water between the neighboring membranes. This is in good agreement with a recent study on DOPC multilayers, where the membrane bending rigidity was reported to be largely independent of the degree of hydration [37]. On the other hand, the intermembrane compression modulus, $B_{\mathrm{bulk}} = 0.9$ MPa, is 20-fold lower than the corresponding value under osmotic stress, $B_{\mathrm{vapor}} = 21$ MPa, which can be attributed to the softer intermembrane confinement in the presence of a water interlayer.

Although it is not a universal feature among all glycolipids, it should be noted that similar sample stabilities in bulk water can be achieved with many synthetic and natural gly-

TABLE II. Parameters of the best matching simulation for Gent-H at 60 °C in bulk D_2O.

System	d (Å)	σ (Å)	η	λ (Å)	R (μm)	κ (J)	κ (k_BT)	B (MPa)
Gent-H	56.8	8.4	0.10	24	1.4	3.2×10^{-20}	7	0.9

colipids. This will enable us not only to physically model biological membranes under physiological conditions but also to study the influence of ions and charged molecules that play key roles in many membrane-associated processes, such as ion-induced cell agglutination [38].

The approach chosen in this study offers a large potential to unravel the unique roles of saccharides in the physical fine-adjustment of interactions at cell-cell contacts, which is complementary to other approaches such as membranes on polymers [39] and membranes on membranes [33].

ACKNOWLEDGMENTS

We thank R. R. Schmidt for his advice in carbohydrate synthesis, D. J. Bicout and E. I. Kats for insightful comments, ILL (Grenoble) for the neutron beam time, and HASYLAB (Hamburg) for the synchrotron beam time. This work has been supported by the Deutsche Forschungsgemeinschaft (Ta259/6) and the Fonds der Chemischen Industrie, R.G.O. and F.R. are thankful to Alexander von Humboldt Foundation for support, and E.S. thanks the State Baden Württemberg for support.

[1] W. D. Comper, *Extracellular Matrix* (Harwood Academic, Amsterdam, 1996).
[2] H. J. Gabius and S. Gabius, *Glycoscience* (Chapmann & Hall, Weinheim, Germany, 1997).
[3] B. Alberts, D. Bray, J. Lewis, M. Raff, K. Roberts, and J. D. Watson, *Molecular Biology of the Cell* (Garland, New York, 1994).
[4] D. A. Pink, L. T. Hansen, T. A. Gill, B. E. Quinn, M. H. Jericho, and T. J. Beveridge, Langmuir **19**, 8852 (2003).
[5] C. R. Safinya, D. Roux, G. S. Smith, S. K. Sinha, P. Dimon, N. A. Clark, and A. M. Bellocq, Phys. Rev. Lett. **57**, 2718 (1986).
[6] C. R. Safinya, E. B. Sirota, D. Roux, and G. S. Smith, Phys. Rev. Lett. **62**, 1134 (1989).
[7] T. Salditt, J. Phys.: Condens. Matter **17**, R287 (2005).
[8] S. Konig, T. M. Bayerl, G. Coddens, D. Richter, and E. Sackmann, Biophys. J. **68**, 1871 (1995).
[9] G. Pabst, J. Katsaras, V. A. Raghunathan, and M. Rappolt, Langmuir **19**, 1716 (2003).
[10] M. C. Rheinstädter, C. Ollinger, G. Fragneto, F. Demmel, and T. Salditt, Phys. Rev. Lett. **93**, 108107 (2004).
[11] N. L. Yamada, H. Seto, T. Takeda, M. Nagao, Y. Kawabata, and K. Inoue, J. Phys. Soc. Jpn. **74**, 2853 (2005).
[12] C. Gege, J. Vogel, G. Bendas, U. Rothe, and R. R. Schmidt, Chem.-Eur. J. **6**, 111 (2000).
[13] M. F. Schneider, G. Mathe, M. Tanaka, C. Gege, and R. R. Schmidt, J. Phys. Chem. B **105**, 5178 (2001).
[14] M. Tanaka, S. Schiefer, C. Gege, R. R. Schmidt, and G. G. Fuller, J. Phys. Chem. B **108**, 3211 (2004).
[15] W. Kern and D. A. Puotinen, RCA Rev. **31**, 187 (1970).
[16] M. Tanaka, F. Rehfeldt, S. S. Funari, C. Gege, and R. R. Schmidt, HASYLAB Annual Report, 2004.
[17] M. F. Schneider, R. Zantl, C. Gege, R. R. Schmidt, M. Rappolt, and M. Tanaka, Biophys. J. **84**, 306 (2003).
[18] See EPAPS Document No. E-PLEEE8-78-035812 for sketches of the climate chamber and the liquid cell, an AFM image and the corresponding height profile of the solid-supported multilayers, and a discussion of the parameter uncertainties. For more information on EPAPS, see http://www.aip.org/pubservs/epaps.html.
[19] L. D. Landau and E. M. Lifshitz, *Statistische Physik Teil 1* (Akademie-Verlag, Berlin, 1987).
[20] B. V. Derjaguin and N. V. Churaev, *Surface Forces* (Consultants Bureau, New York, 1987).
[21] M. Tanaka, F. Rehfeldt, M. F. Schneider, G. Mathe, A. Albersdorfer, K. R. Neumaier, O. Purrucker, and E. Sackmann, J. Phys.: Condens. Matter **17**, S649 (2005).
[22] N. Lei, C. R. Safinya, and R. F. Bruinsma, J. Phys. II **5**, 1155 (1995).
[23] E. A. L. Mol, J. D. Shindler, A. N. Shalaginov, and W. H. de Jeu, Phys. Rev. E **54**, 536 (1996).
[24] S. K. Sinha, J. Phys. III **4**, 1543 (1994).
[25] C. Münster, T. Salditt, M. Vogel, R. Siebrecht, and J. Peisl, Europhys. Lett. **46**, 486 (1999).
[26] V. A. Parsegian, N. Fuller, and R. P. Rand, Proc. Natl. Acad. Sci. U.S.A. **76**, 2750 (1979).
[27] R. P. Rand and V. A. Parsegian, Biochim. Biophys. Acta **988**, 351 (1989).
[28] J. N. Israelachvili, *Intermolecular and Surface Forces* (Academic, London, 1985).
[29] B. Demé, M. Dubois, and T. Zemb, Biophys. J. **82**, 215 (2002).
[30] T. Abraham, S. R. Schooling, M. Nieh, N. Kucerka, T. J. Beveridge, and J. Katsaras, J. Phys. Chem. B **111**, 2477 (2007).
[31] J. F. Nagle and J. Katsaras, Phys. Rev. E **59**, 7018 (1999).
[32] E. Sackmann, in *Structure and Dynamics of Membranes*, edited by R. Lipowski and E. Sackmann (Elsevier, Amsterdam, 1995).
[33] J. Daillant, E. Bellet-Amalric, A. Braslau, T. Charitat, G. Fragneto, F. Graner, S. Mora, F. Rieutord, and B. Stidder, Proc. Natl. Acad. Sci. U.S.A. **102**, 11639 (2005).
[34] M. Tanaka, M. F. Schneider, and G. Brezesinski, ChemPhysChem **4**, 1316 (2003).
[35] M. F. Schneider, K. Lim, G. G. Fuller, and M. Tanaka, Phys. Chem. Chem. Phys. **4**, 1949 (2002).

[36] T. Salditt, M. Vogel, and W. Fenzl, Phys. Rev. Lett. **90**, 178101 (2003).

[37] J. Pan, S. Tristram-Nagle, N. Kucerka, and J. F. Nagle, Biophys. J. **94**, 117 (2008).

[38] I. Eggens, B. Fenderson, T. Toyokuni, B. Dean, M. Stroud, and S. Hakomori, J. Biol. Chem. **264**, 9476 (1989).

[39] M. Tanaka and E. Sackmann, Nature **437**, 656 (2005).